Damage detection and localization on structural connections using vibration-based damage identification methods

振動解析を用いた損傷同定法による構造連結部欠陥の検出と位置決定

Sherif Beskhyroun*, Toshiyuki Oshima**, Shuichi Mikami*** and Tomoyuki Yamazaki****
シェリフ ベスキロウン*, 大島俊之**, 三上修一***, 山崎智之****

*Doctoral Student, Dept. of Civil Eng., Kitami Institute of Technology, (165 Koen-cho, Kitami, 090-8507)
**Professor, Dept. of Civil Eng., Kitami Institute of Technology, (165 Koen-cho, Kitami, 090-8507)
***Asso. Professor, Dept. of Civil Eng., Kitami Institute of Technology, (165 Koen-cho, Kitami, 090-8507)
****Research Asso., Dept. of Civil Eng., Kitami Institute of Technology, (165 Koen-cho, Kitami, 090-8507)

Damage detection based upon changes in vibration characteristics is one of the few methods that can monitor the structure on a global basis. The basic idea of this method is that any changes in the physical properties of the structure (mass, stiffness and boundary conditions) will in turn cause changes in its modal characteristics (resonant frequency, modal damping and mode shapes). In this paper different damage detection methods, based on change in frequency and in mode shapes, have been summarized and applied using experimental and numerical data from steel beam before and after releasing some supporting bolts. Two multi-layer piezoelectric actuators were used for excitation; the advantages of using this technique of excitation are explained. Effectiveness in detecting and localizing the damage is compared for the different damage detection methods.

Key Words: *vibration characteristics, damage detection, modal properties*

1. Introduction

Many aerospace, civil, and mechanical systems continue to be used despite aging and the associated potential for damage accumulation. Therefore, the ability to monitor a structure and detect damage at the earliest possible stage is becoming increasingly important. Damage-detection methods are either visual or localized experimental methods such as acoustic or ultrasonic methods, magnetic field methods, radiograph, eddy-current methods and thermal field methods[1]. These methods can be used only to detect damage near the surface of the structure. Therefore the need for more global damage detection methods that can be applied to complex structure has led to development of methods that examine changes in the vibration characteristics of the structure[2]. Vibration testing can be considered as a global non-destructive health monitoring technique. It can be used in a continuous or intermittent way. In a continuous monitoring system typically a few sensors are installed on the structure whereas a large number of sensors can be used in intermittent monitoring, for example to obtain detailed mode shape information[3]. The basic idea is that modal parameters (frequencies, mode shapes, and modal damping) are a function of the physical properties of the structure (mass, damping, stiffness, and boundary conditions). Therefore, changes in physical properties of the structure, such as its stiffness or flexibility, will cause changes in the modal properties[2),4].

Different damage detection methods, based on the changes in frequency and modal shape, are applied in this paper. Structural damage is determined by using different vibration characteristics. Strain energy distribution of each mode, curvature change of modal shape and change of flexibility matrix are used in different damage detection methods. Those methods are explained in more details in chapter 5. Releasing some of supporting bolts is taken as a damage model on structural connection. Two multi-layer piezoelectric actuators are used for local excitation and acceleration of structural

member is measured and analyzed to find the changes of modal parameters as an effect of structural damage.

2. Measurements by two actuators system

2.1 Experimental equipments

In this research a simple steel beam supported by four bolts in both sides has been examined before and after releasing some bolts as shown in Fig. 1. The multi-layer piezoelectric actuator is used for local excitation. The main advantage of using piezoelectric actuators is that it produces vibration with different frequencies ranging from 0 to 400 Hz that is effective in measuring higher modes. Main characteristics of equipment used in this experiment are shown in Table 1. Oshima et al.[5] have measured and evaluated the location of released bolts by using one excitation actuator system. In this paper we use two actuators excitation system, which has more advantages than one actuator system. Larger amplitude of vibration and more complicated vibration modes will be produced by using multiple actuators in excitation system. Comparison of measured results by one and two actuators as excitation system is shown in this chapter.

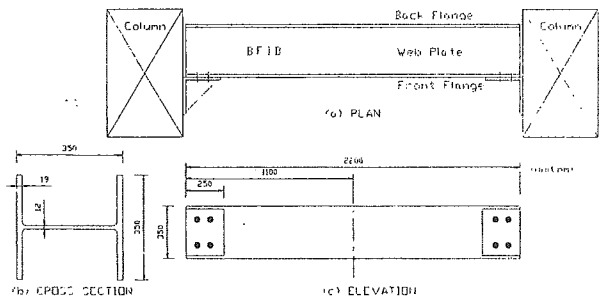

Fig. 1 Beam dimensions

Table 1 Equipment characteristics

Piezoelectric actuator	
Dimensions (W×T×H)	10×10×20(mm)
Min. and Max freq.	0~982Hz
Displacement (100V)	12.3 μ m
Max Force	3500N
Wave function generator	
Min. and Max freq.	0.01 μ Hz~15MHz
Max. Output Volt	20Vp-p/OPEN, ±10V/OPEN

2.2 Comparison of excitation by two actuators and one actuator

In order to compare the arrays of two actuators, five different types of arrays are used as shown in Fig. 2. The two small ellipses on the beam indicate the location of two actuators. And two small rectangles indicate the location of accelerometers. In Fig. 2 the location of released bolts is shown and white circles are released bolts.

Power Spectrum Density of acceleration data at the same channel is shown in Fig. 3. In this figure, dot line indicates PSD when one actuator is used for excitation and the solid line indicates PSD when two actuators are used for excitation. By using two actuators excitation, higher amplitudes and more sharp peaks at resonant frequencies are obtained as shown in the same figure. Comparison of peak frequencies by one and two actuators excitation is shown in Table 2. Results are shown on 11^{th}, 12^{th} and 13^{th} modes on vibration only for Case A, Case B and Case C and it is obtained by FFT on the accelerometer data No.1 located as shown in Fig. 2. Data of one actuator excitation is obtained in the paper by Oshima et al.[5] and actuator is located at span center of beam and lower position on front flange surface. By the comparison between one and two actuators stable results are obtained on each results by two actuators excitation. From wave function generator through power source equipment same electrical waves are input on two actuators and duplicated excitation forces are induced on the structure and signal/noise ratio is much improved. If we could coordinate the array of actuators to be more sophisticated excitation we will identify the location and level of damage more precisely by analyzing response wave in both frequency and time domain.

2.3 Measurement of mode shapes and resonant frequencies for undamaged and damaged structure.

The main objective in this section is to determine different mode shapes and resonant frequencies for the beam before and after each case of damage. The measured mode shapes and frequencies before and after each case of damage will be compared using different damage identification methods in order to detect and localize small types of damage. Two cases of damage are introduced to the left support of the beam. Case 0 represents the undamaged beam, Case 1 represents one bolt released, the upper right bolt from the left support, and Case 2 after releasing two bolts, the upper right and the lower right bolts as shown in Fig. 4.

Two piezoelectric actuators having the same waveform were used for excitation. Nine accelerometers and one reference accelerometer were used to measure the beam response. Position of actuators and accelerometers is shown in Fig. 5. Cross power spectrum for the measured acceleration between one reference channel and different measuring points are calculated. Mode shapes were determined from amplitude and phase information contained in CPS of the various accelerometer readings relative to the reference accelerometer. Resonant frequencies and mode shapes are measured for the undamaged beam as well as for each case of damage and these data will be used in the different damage identification methods.

3. Numerical model

The finite element model of the actual beam is created using Structural Analysis Program, SAP2000. The model is benchmarked against the measured frequencies of the actual beam[2),6)]. In order to fix

the numerical value of spring stiffness as a model of bolt, numerical simulation was repeated to agree with the result of experimental

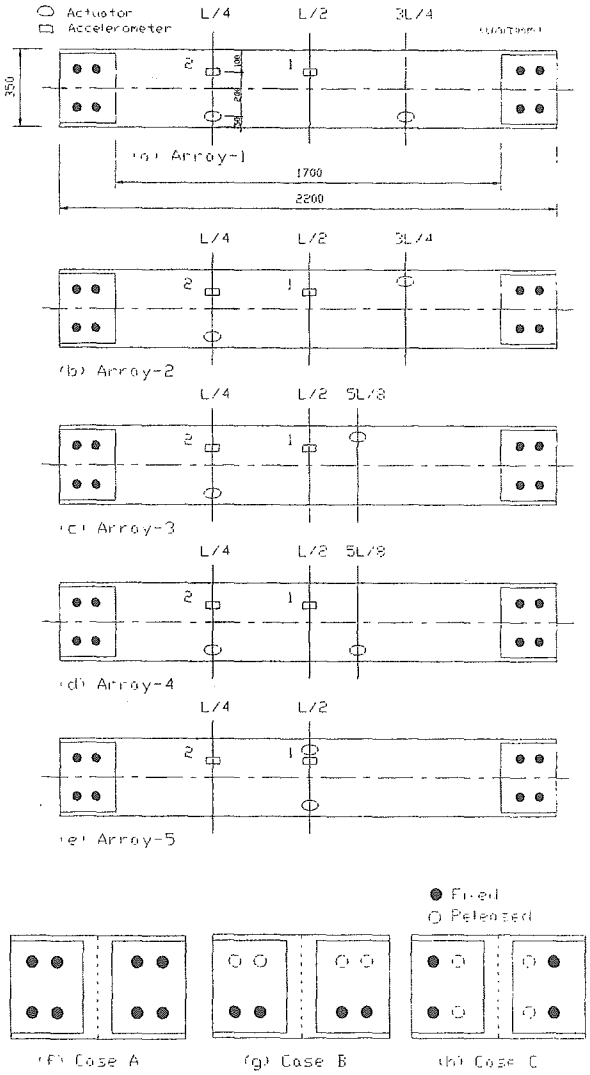

Fig. 2 Actuators array and cases of bolt release

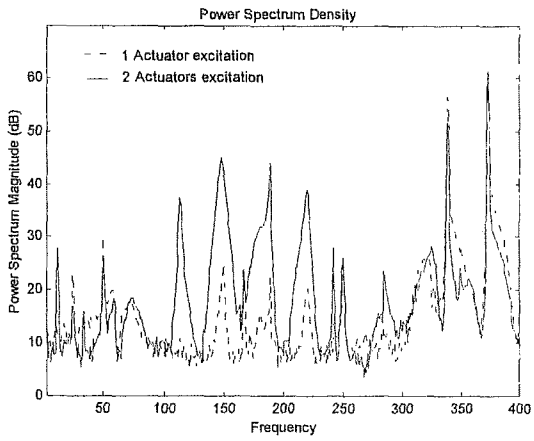

Fig. 3 PSD using one and two actuators excitation

frequency. At each support, springs are divided to three groups, (Fig. 6b), each of them has the same stiffness value and rotational degrees of freedom are restrained at each spring. Spring stiffness values for each group are shown in Table 3. Case 1 of damage is simulated by removing the springs in all directions X, Y, and Z at the upper 4 nodes of group C as shown in Fig. 6b and Case 2 is simulated similarly

Table 2 Frequency comparison between one and two actuators excitation system for five array types

	Mode	One actuator	Two actuators, Array types				
			1	2	3	4	5
Case A	11	328.8	329.2	329.3	329.4	329.5	328.5
	12	337.9	338.5	338.5	338.5	338.5	338.4
	13	372.7	373.2	373.2	373.3	373.3	373.2
Case B	11	316.9	321.1	321.2	321.3	321.1	320.9
	12	334.2	335.5	335.3	335.2	335.3	335.2
	13	365.7	367.9	367.9	367.9	367.9	367.8
Case C	11	323.5	326.0	325.7	326.0	325.7	325.9
	12	338.0	336.1	336.1	336.0	336.1	335.9
	13	368.2	369.6	369.5	369.5	369.5	369.4

(Hz)

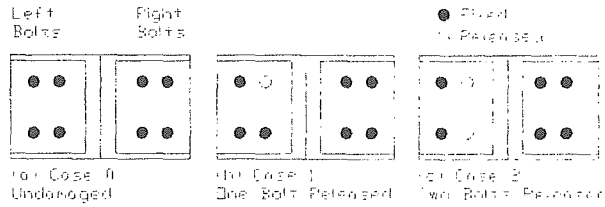

Fig. 4 Damage cases

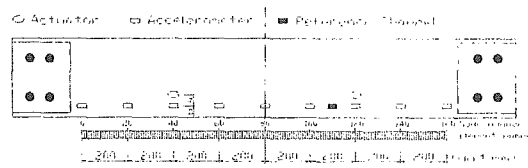

Fig. 5 Actuators and accelerometers positions removing the springs

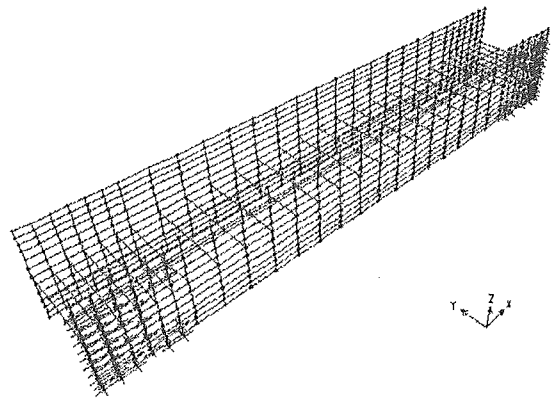

(a) Numerical model for the beam

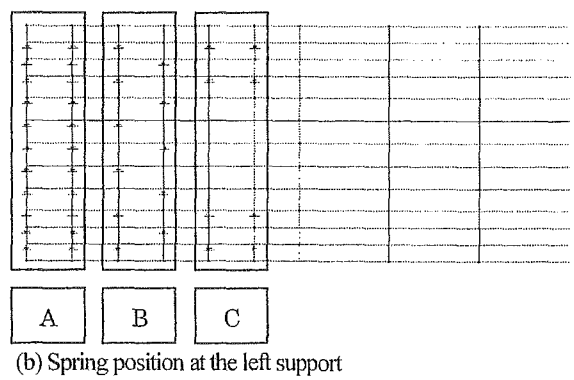

(b) Spring position at the left support

Fig. 6 Numerical model and position of springs at the left support

by removing all springs at group C. Rotational degrees of freedom in all directions are released at the removed springs. Mode shapes and frequencies given by the numerical model before and after each case of damage will be compared using the same damage identification methods in order to compare the results of the damage detection methods for both experimental and numerical data. The numerical model can be used to introduce more damage cases.

Table 3 Spring stiffness at the beam support

	K_x	K_y	K_z
Group A	100	37.5	100
Group B	85	20	85
Group C	80	15	80

(KN/mm)

4. Damage detection methods based on change in frequency

4.1 Percentage of difference in frequency before and after damage

Table 4 shows the change in frequency in the numerical model after each case of damage. It is apparent that change in frequency is very small even after introducing the second level of damage. The remarkable change occurs at mode 10 for both cases of damage since this mode is vertical (in Z direction) and it is the most sensitive for releasing any bolts. The previous result indicates that some modes are more sensitive for each type and position of damage; therefore it is very important to measure these modes experimentally in order to detect this type of damage in the actual structure. The numerical model can be used to determine the most sensitive modes for different types and positions of damage.

Table 4 Change in resonant frequency for numerical model

Mode No.	Frequency (Hz)				
	Case 0	Case 1	% Diff.	Case 2	% Diff.
1	25.10	25.07	-0.10	25.05	-0.20
2	41.82	41.80	-0.04	41.78	-0.08
3	116.17	116.07	-0.09	115.94	-0.20
4	149.95	149.90	-0.04	149.84	-0.08
5	174.58	174.42	-0.09	174.19	-0.22
6	205.12	204.93	-0.09	204.67	-0.22
7	216.23	214.32	-0.89	212.37	-1.82
8	249.37	249.25	-0.05	249.13	-0.10
9	281.60	281.52	-0.03	281.42	-0.06
10	306.84	301.57	-1.75	293.93	-4.39
11	329.83	327.52	-0.70	325.73	-1.26
12	346.48	346.36	-0.03	346.25	-0.06
13	379.57	379.21	-0.09	378.95	-0.16

4.2 Frequency spectrogram

The second method for comparing the change in resonant frequency is using Gabor spectrogram. In this spectrogram the frequency components at each time are plotted using colored spectrum. Figs. 7, 8 and 9 show Gabor spectrogram for experimental data for Case 0, Case 1 and Case 2, respectively. Very small change is observed only for Case 2 of damage as shown on the circled area.

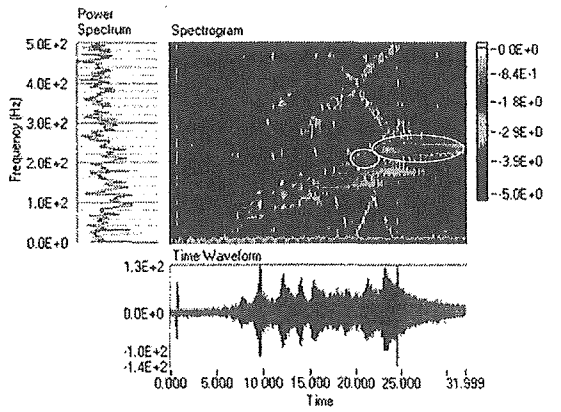

Fig. 7 Gabor spectrogram for Case 0 (experimental data)

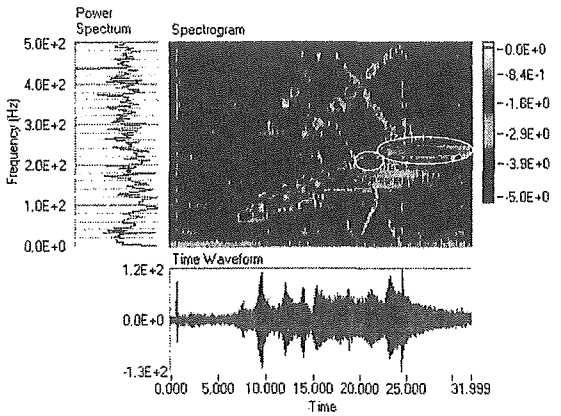

Fig. 8 Gabor spectrogram for Case 1 (experimental data)

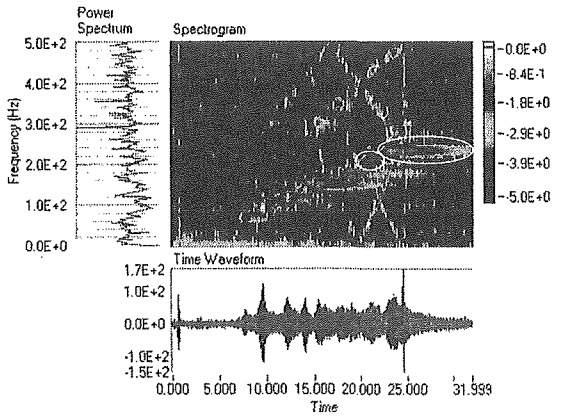

Fig. 9 Gabor spectrogram for Case 2 (experimental data)

These very small changes in frequency for both experimental and numerical data has led to the conclusion that damage detection methods based on change in frequency are not sensitive for detecting the damage. In the following chapter damage detection methods, which are based on change in mode shape, will be examined using experimental and numerical data.

5. Damage detection methods based on change in mode shape.

where E = the modulus of elasticity and I = the moment of inertia of the section. From Eq. (7), it is shown that the curvature of the beam is proportional to the inverse of the stiffness for a given moment. Therefore for the same moment applied to the structure before and after damage, any reduction in the stiffness of the structure associated with damage will increase the curvature. Furthermore, the amount of change in the mode shape curvature is proportional to the level of damage. Higher level of damage, which means larger reduction in stiffness, will lead to larger change in curvature. Maximum difference in mode shape curvature before and after damage indicates the position of damage.

(3) Change in flexibility method

Flexibility matrix, [F], of a structure may be expressed in terms of modal parameters as follows[2), 4), 10)]

$$[F] \approx [\Phi][\Omega]^{-1}[\Phi]^T \approx \sum_{i=1}^{n} \frac{1}{\omega_i^2} \{\phi_i\}\{\phi_i\}^T \quad (8)$$

where $\{\phi_i\}$ = the i^{th} mass-normalized mode shape, $[\Phi]$ = the mode shape matrix= $[\phi_1, \phi_2, \ldots \phi_n]$, (ω_i) = the i^{th} modal frequency, $[\Omega]$ = the modal stiffness matrix = diag. (ω_i^2), and n = the number of measured or calculated modes.

Similarly, for the damaged structure

$$[F^*] \approx [\Phi^*][\Omega^*]^{-1}[\Phi^*]^T \approx \sum_{i=1}^{n} \frac{1}{(\omega_i^*)^2} \{\phi_i^*\}\{\phi_i^*\}^T \quad (9)$$

where the asterisks signify properties of the damaged structure. Flexibility of a point k may be interpreted as a measure of the energy in a structure due to a unit load at node k. Hence, variation of flexibility coefficients in the neighborhood of a node k may reveal damage localized in its vicinity[11)]. Therefore the change in flexibility caused by the damage can be obtained as follows

$$[\Delta F] = [F] - [F^*] \quad (10)$$

where ΔF represents the change in flexibility matrix. Now, for each column of matrix ΔF let δ_j be the absolute maximum value of the elements in the j^{th} column. Hence,

$$\delta_j = \max|\delta_{ij}|, \; i = 1,\ldots n \quad (11)$$

where δ_{ij} are elements of matrix ΔF and n is the number of degrees of freedom. The degree of freedom corresponding to the maximum value of δ_j indicates the position of damage.

(4) Change in uniform load surface curvature method

In this method certain aspects of the mode shape curvature method and change in flexibility method are combined[2), 4), 12)]. In this method the change in curvature is obtained from the uniform flexibility shape instead of the mode shapes. Recall that the flexibility matrices, before and after damage, can be expressed in terms of modal parameters as:

$$[F] \approx [\Phi][\Omega]^{-1}[\Phi]^T \approx \sum_{i=1}^{n} \frac{1}{\omega_i^2} \{\phi_i\}\{\phi_i\}^T \quad (12)$$

and

$$[F^*] \approx [\Phi^*][\Omega^*]^{-1}[\Phi^*]^T \approx \sum_{i=1}^{n} \frac{1}{(\omega_i^*)^2} \{\phi_i^*\}\{\phi_i^*\}^T \quad (13)$$

where the asterisks designate the damaged structure. The coefficients of the i^{th} column in the flexibility matrix represent the deflected shape assumed by the structure with a unit load applied at the i^{th} degree of freedom. Change in curvature of the uniform load flexibility is used to determine the location of damage. The uniform load flexibility represents the deflected shape assumed by the structure when all degrees of freedom are loaded with a unit load. Thus, the uniform load flexibility corresponds to the sum of the unit load flexibilities. In terms of the unit load flexibilities, the curvature change is evaluated as follows

$$\{\Delta\} = \sum_{i=1}^{n} \left| \{F_i^{*''}\} - \{F_i''\} \right| \quad (14)$$

where $\{\Delta\}$ and n represent the absolute curvature change and the number of degrees of freedom, respectively. The degree of freedom corresponding to the maximum value of $\{\Delta\}$ indicates the position of damage.

5.3 Damage identification methods applied to experimental data

Different mode shapes of the beam are measured at nine points as was explained in section 2.3. Interpolation between the measured points using cubic polynomial has been made to approximate mode shape amplitudes between sensors. This interpolation introduces artificial degrees of freedom into the experimental data[2)]. By using this technique, the beam was divided into 160 nodes starting from the first left accelerometer as shown in Fig.5. Figs. 10 through 17 show the results from different damage identification methods when they are applied to experimental data.

In Fig. 10, damage index exceeds the value of two at elements 40 and 120, which indicates the occurrence of damage. Position 40 is close to the damage position but position 120 is false position. When the same method is applied to case 2, it was noticed that the damage index value increased at element 40 but decreased at element 120 which indicate false results at element 120. Therefore when this method is applied in a continuous manner to monitor the structure, continuous increase of damage index, over the value of two, at the same element may ensure the existence of damage at that element. For the change in mode shape curvature method, the maximum change occurs at nodes 100 and 120 and the absolute difference in curvature increases with the increase of damage as shown in Fig. 12 and 13, respectively. The same remarks are obtained for change in flexibility method and change in flexibility shape curvature method as

shown in Figs. 14 to 17. From the previous results, the following remarks are concluded:

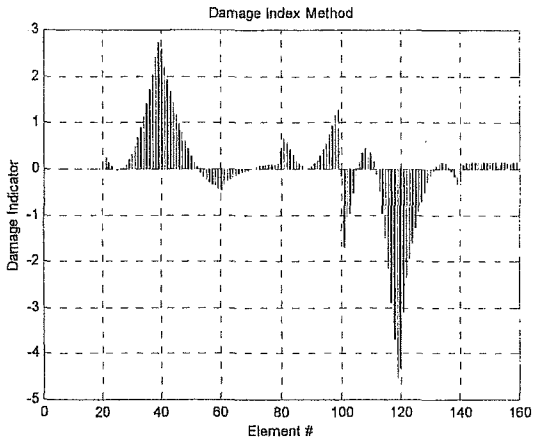

Fig. 10 Damage index method applied to experimental data for damage Case 1.

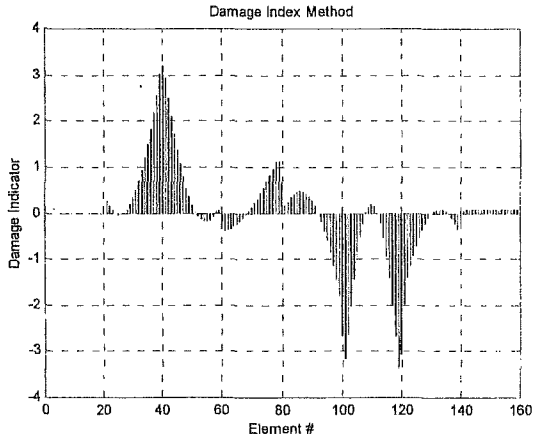

Fig. 11 Damage index method applied to experimental data for damage Case 2.

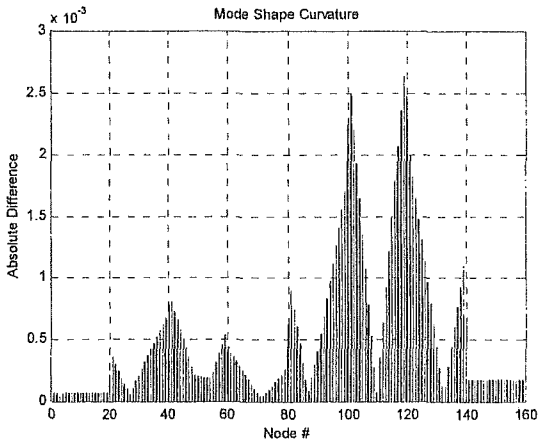

Fig. 12 Mode shape curvature method applied to experimental data for damage Case 1.

1) These methods are more sensitive in measuring changes in modal characteristics due to damage than observing the change in resonant frequency.
2) All methods indicated the existence of damage from the first case of damage but the accuracy of localizing damage position need to be improved.

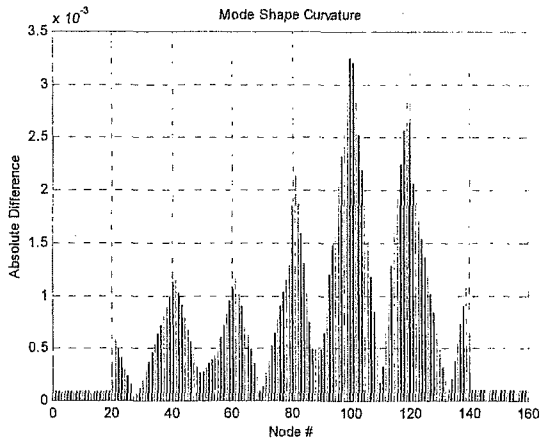

Fig. 13 Mode shape curvature method applied to experimental data for damage Case 2.

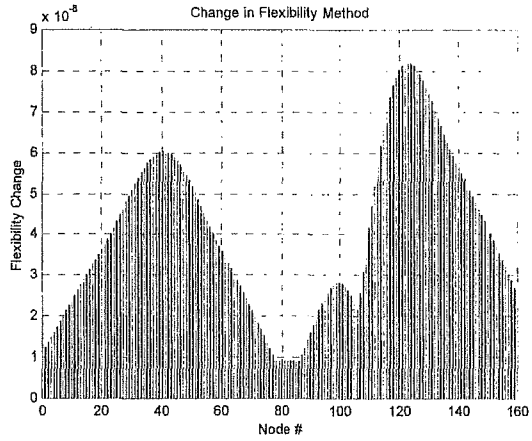

Fig. 14 Change in flexibility method applied to experimental data for damage Case 1.

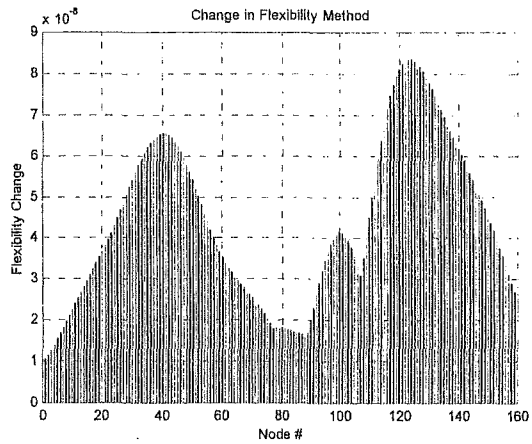

Fig. 15 Change in flexibility method applied to experimental data for damage Case 2.

5.1 Modal assurance criterion (MAC)

Modal assurance criterion[2),4),7)] compares two modes using the orthogonality properties of the mode shapes. The MAC that compares mode i and j has the form

$$MAC(i,j) = \frac{\left|\sum_{k=1}^{n}(\phi_j)_k(\phi_i)_k^*\right|^2}{\left[\sum_{k=1}^{n}(\phi_j)_k(\phi_j)_k^*\right]\left[\sum_{k=1}^{n}(\phi_i)_k(\phi_i)_k^*\right]} \quad (1)$$

where $(\phi)_k$ is an element of the mode-shape vector and the asterisk denotes complex conjugate. In practice, MAC value greater than 0.9 indicates correlated modes and value less than 0.05 indicates uncorrelated modes. MAC was used to compare mode shapes before and after each case of damage. Therefore MAC value for the same mode before and after damage less than 0.9 indicates the existence of damage but it cannot locate the position of damage.

Table 5 shows MAC values between each case of damage and the undamaged case for numerical and experimental data. It is shown that no significant change in MAC values except for mode 10 in both cases of damage, which again signifies the sensitivity of mode 10 for that type of damage.

Table 5 MAC comparison for numerical and experimental data

Mode No.	MAC (Numerical data)		MAC (Experimental data)	
	C.0 & C.1	C.0 & C.2	C.0 & C.1	C.0 & C.2
1	1.0000	0.9999	N/A	N/A
2	0.9999	0.9996	N/A	N/A
3	1.0000	1.0000	N/A	N/A
4	0.9992	0.9985	N/A	N/A
5	1.0000	1.0000	0.9746	0.9621
6	1.0000	0.9998	N/A	N/A
7	0.9998	0.9990	0.9978	0.9954
8	0.9999	0.9999	0.9548	0.9499
9	1.0000	0.9998	0.9970	0.9941
10	0.9176	0.2578	0.9255	0.8633
11	0.9965	0.9950	N/A	N/A
12	0.9998	0.9998	0.9851	0.9758
13	0.9990	0.9998	0.9970	0.9965

5.2 Damage identification algorithms based on change in mode shape.

There are some damage identification methods as listed in references. Comparison of applied results to our experimental data by using those identification methods is dealt with in this paper.

At the fixed support no response can be measured even after releasing few bolts, therefore the applicability of different damage detection methods to detect and localize such type of damage will be examined and compared.

In this section a brief summary of each method will be summarized. For a more detailed summary the reader is referred to the cited references.

(1) Damage index method

This method [2), 4), 8)] is used to detect and locate damage in structures using mode shapes before and after damage. For a structure that can be represented as a beam, a damage index β is developed based on the change in strain energy stored in the structure when it deforms in its particular mode shape. For location j on the beam this change in the i^{th} mode strain energy is related to the change in curvature of the mode at location j. The damage index for this location and this mode, β_{ij}, is defined as

$$\beta_{ij} = \frac{(\int_a^b [\psi_i^{*''}(x)]^2 dx + \int_0^L [\psi_i^{*''}(x)]^2 dx)\int_0^L [\psi_i''(x)]^2 dx}{(\int_a^b [\psi_i''(x)]^2 dx + \int_0^L [\psi_i''(x)]^2 dx)\int_0^L [\psi_i^{*''}(x)]^2 dx} \quad (2)$$

where $\psi''(x)$ $\psi^{*''}(x)$ are the second derivative of i^{th} mode shape corresponding to the undamaged and damaged structure, respectively. L is beam length and a, b are the limits for element j. When more than one mode is used, damage index is defined as the sum of damage indices from each mode as follows

$$\beta_j = \sum_{i=1}^{n} \beta_{ij} \quad (3)$$

where n is the number of modes.

Assuming that the collection of the damage indices, β_j, represents a sample population of a normally distributed random variable, a normalized damage localization indicator is obtained as follows

$$Z_j = \frac{\beta_j - \overline{\beta_j}}{\sigma_j} \quad (4)$$

where $\overline{\beta_j}$ and σ_j represent the mean and standard deviation of the damage indices, respectively. A statistical decision making procedure is employed to determine if the normalized damage index, Z_j, is associated with a damage location. Values of two standard deviations from the mean are assumed to be associated with damage locations.

(2) Mode shape curvature method

In formulating the eigenvalue problem, i.e. Eq. (5), structural damage only affects the stiffness matrix and not the mass matrix[2),4),9)]. For the undamaged condition the eigenvalue problem is given as

$$([K] - \lambda_i[M])\{x_i\} = \{0\} \quad (5)$$

where [K] = the stiffness matrix, λ_i = the i^{th} eigenvalue, [M] = the mass matrix, and $\{x_i\}$ = the i^{th} displacement eigenvector.

Similarly, the eigenvalue problem for the damaged condition is

$$([K^*] - \lambda_i^*[M])\{x_i^*\} = \{0\} \quad (6)$$

where the asterisks signify properties of the damaged structure. Eigenvectors for the damaged and undamaged structure are the basis for damage detection. For a beam cross section subjected to a bending moment M(x), the curvature at location x, $v''(x)$, is given by

$$v''(x) = M(x)/EI \quad (7)$$

3) Continuous increase of the damage measure at the same position may ensure the location of damage at that position, on the other hand fluctuating results at the same position may indicate false position of damage.
4) Damage index method showed the best results among the different methods in localizing the damage position.

These results will be verified using the numerical data extracted from the finite element model.

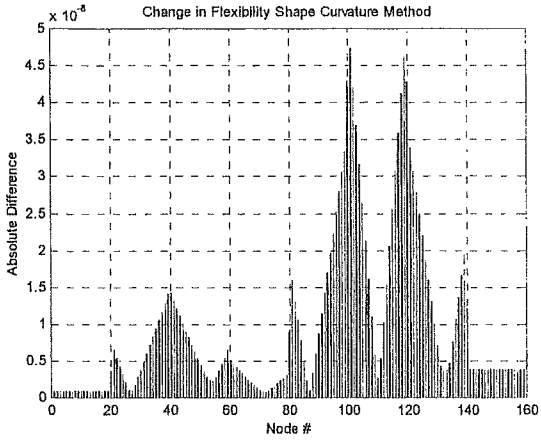

Fig. 16 Change in flexibility shape curvature method applied to experimental data for damage Case 1.

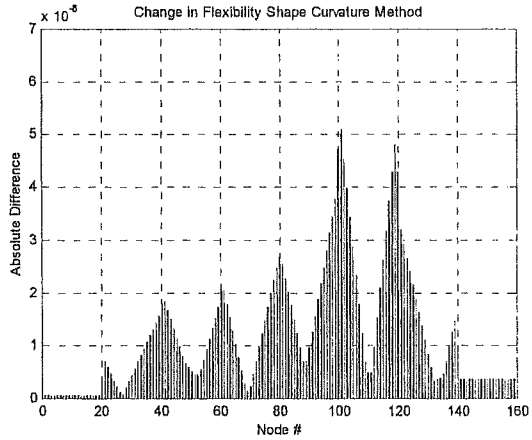

Fig. 17 Change in flexibility shape curvature method applied to experimental data for damage Case 2.

5.4 Damage identification methods applied to numerical data

Similar to experimental data, mode shapes were measured along nine points on the front flange, and then interpolation between the measured points using cubic polynomial has been made to approximate mode shape amplitudes between the measured points. Therefore the beam is also divided into 160 nodes. Figs. 18 through 25 show the results from different damage identification methods when they are applied to numerical data. In Figs. 18 and 19, damage index exceeds the value of two at element 20 for case 1 and case 2. The measured position of damage, indicated by damage index method, is very close to the actual position of damage in both cases of damage and no false positions of damage were measured. In Figs. 20 and 21, mode shape curvature method showed poor results in indicating the damage position and the decrease in absolute difference from case 1 to case 2 indicates that the measured positions of damage may be false positions. For both change in flexibility method and change in flexibility shape curvature method, the position of damage is determined accurately only at case 2 of damage as shown in Figs. 23 and 25, respectively. Comparing Fig. 24 with Fig. 25, the absolute

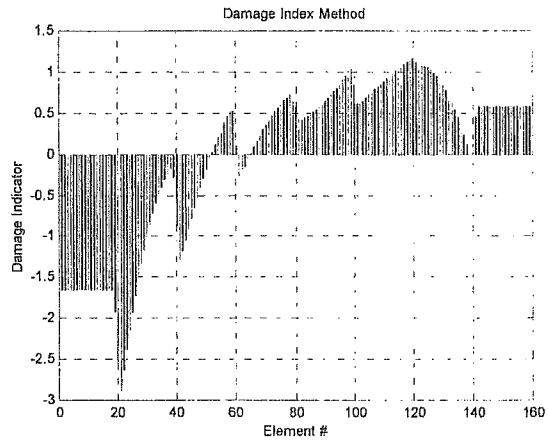

Fig. 18 Damage index method applied to numerical data for damage Case 1.

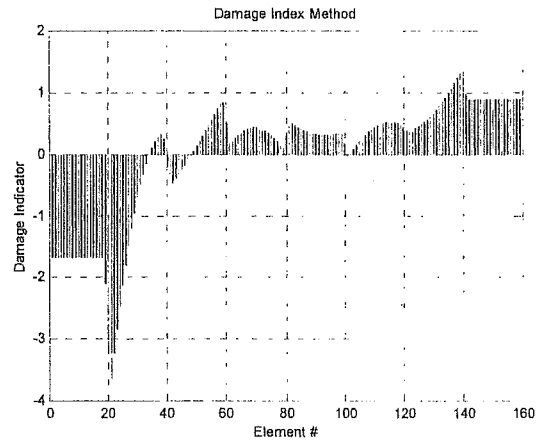

Fig. 19 Damage index method applied to numerical data for damage Case 2.

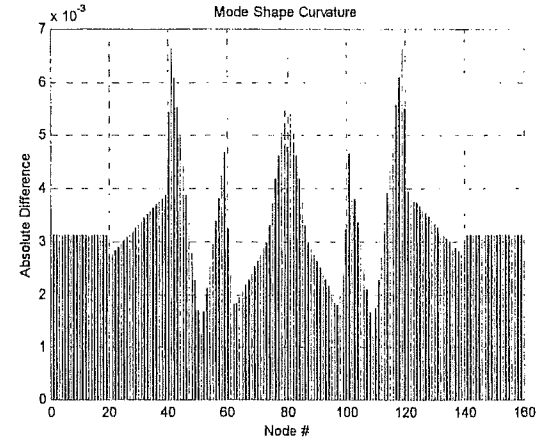

Fig. 20 Mode shape curvature method applied to numerical data for damage Case 1.

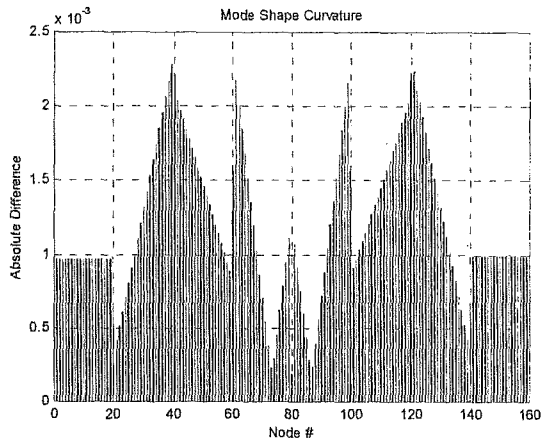

Fig. 21 Mode shape curvature method applied to numerical data for damage Case 2.

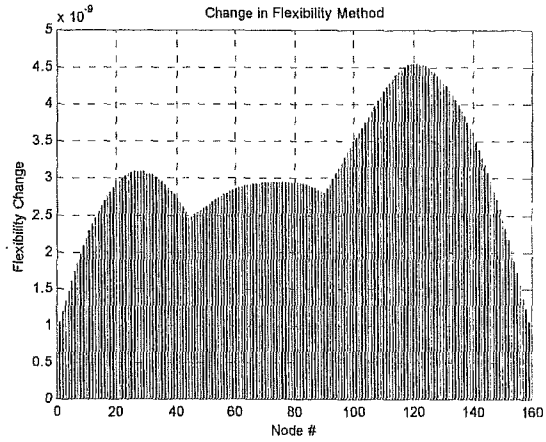

Fig. 22 Change in flexibility method applied to numerical data for damage Case 1.

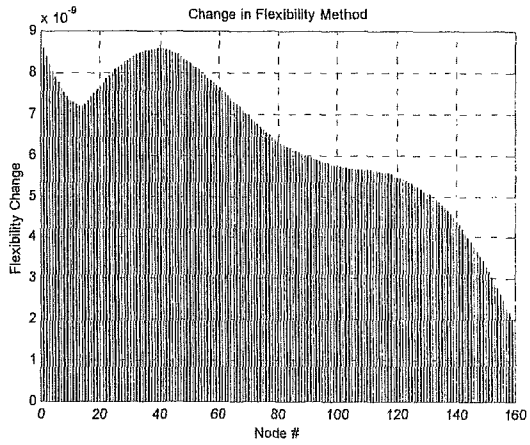

Fig. 23 Change in flexibility method applied to numerical data for damage Case 2.

difference decreased at element 120 from case 1 to case 2 which indicate that the measured position at that element in case 1 was false position.

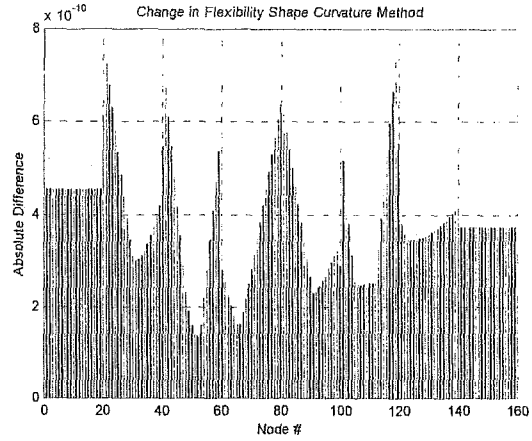

Fig. 24 Change in flexibility shape curvature method applied to numerical data for damage Case 1.

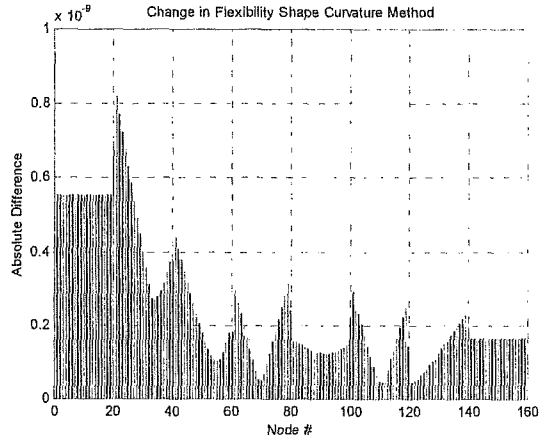

Fig. 25 Change in flexibility shape curvature method applied to numerical data for damage Case 2.

5.5 Damage position as indicated by different methods

Table 6 summarizes the position of damage as indicated by different damage methods for experimental and numerical data for both cases of damage. It is observed that the numerical results are consistent with the experimental results and damage position is determined more accurately for the numerical data, which ensures the accuracy of the numerical model. Therefore, the finite element model can be used to produce different damage types, positions and sizes of damage and hence the results of different damage identification methods for each type of damage are obtained. These results can be used to estimate the type and position of damage from the results of the actual structure. Damage index method has shown the best results in detecting and localizing the damage from the first case of damage and for both experimental and numerical data.

Table 6 Damage position as indicated by different damage methods*)

Damage method	Dam. position (Exp. data)		Dam. position (Num. data)	
	Case 1	Case 2	Case 1	Case 2
Damage index	40, 120	40, 100, 120	20	20
Mode shape curavature	100, 120	100, 120	40, 120	40, 120
Change in flexibility	40, 120	40, 120	120	0, 40
Uniform load surface curvature	100, 120	100, 120	20, 120	20

*) Number in table indicates node number or element number

6. Concluding remarks

(1) Using multi-layer piezoelectric actuator for excitation is more effective in measuring higher modes than the other methods such as impulse hammer or electronic shaker.

(2) Using two multi-layer piezoelectric actuators, having the same electrical wave function, has shown better results in measuring mode shapes and frequencies and in improving the signal/noise ratio.

(3) There are always some modes, which are more sensitive for each type and position of damage than the other modes. It is, therefore, important to measure these modes for the real structure in order to improve the ability of detecting that type of damage.

(4) Examining the change in resonant frequency due to damage either by using the percentage of difference in frequency or using frequency spectrogram, low sensitivity for damage detection is obtained.

(5) Damage detection methods, which are based on change in mode shapes, are more sensitive in detecting damage than observing the change in resonant frequency.

(6) Damage index method has shown the best results among the different methods in detecting and localizing the damage.

(7) Finite element model for the actual structure can be used to produce many different patterns, sizes and positions of damage and hence appropriate damage identification methods should be chosen for each type of damage. These results can be used to estimate the type and position of damage from the results of the actual structure.

Acknowledgement

This research is supported by the Grant-in-Aids for Scientific Research, Ministry of Education. The authors wish to thank for this support.

References

1) Doebling S. W., C. R. Farrar, M. B. Prime, and D. W. Shevitz, *Damage Identification and Health Monitoring of Structural and Mechanical Systems from Changes in their Vibration Characteristics*, A Literature Review, Los Alamos National Laboratory Report, LA-13070- MS, 1996.

2) Farrar C. R. and D. A. Jauregui, *Damage Detection Algorithms Applied to Experimental and Numerical Model Data from the I-40 Bridge*, Los Alamos National Laboratory Report, LA-12979-MS, 1996.

3) Peeters B., Maeck J. and De Roeck G., Vibration-based damage detection in civil engineering: excitation sources and temperature effects, *Smart Mater. Struct.* 10 pp.518-527, 2001.

4) Farrar C. R. and D. A. Jauregui, Comparative study of damage identification algorithms applied to a bridge: I. Experiment, *Smart Mater. Struct.* 7 pp.704-719, 1998.

5) Oshima T. et al., Study on damage evaluation of joint in steel member by using local vibration excitation, *Journal of Applied Mechanics*, Vol.5, pp.837-846, 2002.

6) Farrar, C. R. and D. A. Jauregui, Comparative study of damage identification algorithms applied to a bridge: II. Numerical study, *Smart Mater. Struct.* 7 pp.704-719, 1998.

7) Ewins D. J., *Modal Testing: Theory and Practice*, John Wiley, New York, 1985.

8) Stubbs N., J. T. Kim, and C. R. Farrar, Field Verification of a Nondestructive Damage Localization and Sensitivity Estimator Algorithm, *Proceedings of the 13th International Modal Analysis Conference*, pp. 210-218, 1995.

9) Pandey A. K., Biswas M. and Samman M. M., Damage detection from changes in curvature mode shapes, *J. Sound Vib.* 145 pp.321-332, 1991.

10) Pandey A. K., Biswas M., Damage detection in structures using changes in flexibility, *J. Sound Vib.* 169 pp.3-17, 1994.

11) Raghavendrachar M. and Aktan A. E., Flexibility by multireference impact testing for bridge diagnostics, *Structural Engineering*, Vol. 118, No.8, pp.2186-2203, 1990.

12) Zhang Z. and Aktan A. E., The damage indices for the constructed facilities, *Proc. 13th Int. Modal Analysis Conf.* Vol 2, pp.1520-1529, 1995.

(Received: April 18, 2003)